A revised model of the inner-hair cell and auditory-nerve complex

Christian J. Sumner[a)]
Centre for the Neural Basis of Hearing at Essex, Department of Psychology, University of Essex, Colchester CO4 3SQ, United Kingdom

Enrique A. Lopez-Poveda
Centro Regional de Investigación Biomédica, Facultad de Medicina, Universidad de Castilla-La Mancha, Campus Universitario, 02071 Albacete, Spain

Lowel P. O'Mard and Ray Meddis
Centre for the Neural Basis of Hearing at Essex, Department of Psychology, University of Essex, Colchester CO4 3SQ, United Kingdom

(Received 23 April 2001; revised 1 November 2001; accepted 31 December 2001)

A revised computational model of the inner-hair cell (IHC) and auditory-nerve (AN) complex is presented and evaluated. Building on previous models, the algorithm is intended as a component for use in more comprehensive models of the auditory periphery. It combines smaller components that aim to be faithful to physiology in so far as is practicable and known. Transduction between cochlear mechanical motion and IHC receptor potential (RP) is simulated using a modification of an existing biophysical IHC model. Changes in RP control the opening of calcium ion channels near the synapse, and local calcium levels determine the probability of the release of neurotransmitter. AN adaptation results from transmitter depletion. The exact timing of AN action potentials is determined by the quantal and stochastic release of neurotransmitter into the cleft. The model reproduces a wide range of animal RP and AN observations. When the input to the model is taken from a suitably nonlinear simulation of the motion of the cochlear partition, the new algorithm is able to simulate the rate-intensity functions of low-, medium-, and high-spontaneous rate AN fibers in response to stimulation both at best frequency and at other frequencies. The variation in fiber type arises in large part from the manipulation of a single parameter in the model: maximum calcium conductance. The model also reproduces quantitatively phase-locking characteristics, relative refractory effects, mean-to-variance ratio, and first- and second-order discharge history effects. [DOI: 10.1121/1.1453451]

PACS numbers: 43.64.Bt, 43.66.Ba [LHC]

I. INTRODUCTION

The inner-hair-cell (IHC) and auditory-nerve (AN) complex is the primary apparatus for the transduction of basilar membrane (BM) motion into neural signals. Because transduction is an obligatory stage in the auditory pathway, computational models of IHCs are a vital component in any auditory modeling project. Here, we present a revised version of an earlier IHC model (Meddis, 1986, 1988; Meddis *et al.*, 1990) that improves on previous models in terms of the range of phenomena simulated and is more consistent with recent developments in hair-cell physiology.

IHCs have been the subject of modeling studies for at least three decades (e.g., Davis, 1965; Weiss, 1966). The goals of the research have been varied. Many models focus on possible mechanisms for adaptation (e.g., Schroeder and Hall, 1974; Smith and Brachman, 1982; Eggermont, 1985; Meddis, 1986). Others are concerned with the biophysics of hair cells (e.g., Shamma *et al.*, 1986; Rattay *et al.*, 1998) or the mechano-electric transduction process (Corey and Hudspeth, 1983). The purpose of the model to be described below is primarily to generate an accurate representation of the input–output characteristics of the hair cell for arbitrary stimuli. Physiological accuracy, for its own sake, is a lesser concern. However, inclusion of key physiological processes (as far as these are known) is likely to be a productive strategy and this is the approach that is adopted below.

Many older models (e.g., Meddis, 1986; Carney, 1993) simulate the response of high-spontaneous rate (HSR) fibers to pure tones at the fiber's best frequency (BF). However, they make no specific claim to represent the response of medium (MSR) and low (LSR) spontaneous rate fibers, nor do they claim to deal with pure-tone responses for frequencies away from BF. It is clear from AN measurements that the characteristics of MSR and LSR fiber types are strongly influenced by nonlinear aspects of mechanical filtering (Yates *et al.*, 1990). The same nonlinearities can also explain why the shape of rate-intensity (RI) functions for a single AN fiber does vary considerably with stimulating frequency. The new model simulates these effects by including a nonlinear model of the response of the BM as the input to the hair cell. This study joins several recent reports that address the modeling of nonlinear filtering (Robert and Erikson, 1999; Irino and Patterson, 2001; Zhang *et al.*, 2001). How-

[a)]Current address: Kresge Hearing Research Institute, University of Michigan, Ann Arbor, 48109-0506. Electronic mail: cjsumner@umich.edu

ever, we emphasize the development of the IHC model and its rate responses to pure-tone stimuli. The response to complex stimuli will be reported elsewhere. Also, the testing of the model is restricted wherever possible to guinea-pig data at high BFs.

An earlier version of the new model (Lopez-Poveda *et al.*, 1998) used an existing biophysical model of the IHC receptor potential (RP) (Davis, 1965; Shamma *et al.*, 1986), to control the synaptic adaptation stage from the original Meddis IHC model. They simulated the control relationship between the RP and the transmitter release probability as an exponential function, and were able to reproduce the characteristic input/output functions associated with HSR, MSR, and LSR fibers. However, the exponential function led to unrealistically high release rates at high stimulus levels. Schoonhoven *et al.* (1997) employed a similar model but found a saturating exponential to be a more suitable function. Recently, Robert and Erikson (1999) have employed a quadratic function for the same purpose. In the new model, we hypothesize that a single presynaptic calcium current controls the rate of transmitter release and have explicitly modeled this process. Calcium currents are necessary for neurotransmitter release at all chemical synapses (Augustine *et al.*, 1985a). These have the advantage of offering a naturally saturating, exponential function. We find that variations in maximum calcium conductance can be successfully used to change the fiber response from low- through to high-spontaneous rate type of RI function.

The new model uses a previous simulation of the circulation of transmitter at the synapse (Meddis, 1986) but the release of neurotransmitter is now quantal and stochastic. Further, the release of a single quantum of transmitter is assumed to initiate an action potential (AP) in the postsynaptic AN fiber, if it is not already in a refractory state. This idea was suggested by Geisler (1981), and is supported by observations of postsynaptic potentials (Siegel, 1992). Thus, the stochastic nature of AP generation in AN fibers is treated as *synaptic* in origin. This stochastic release leads to first- and second-order discharge history effects. Postsynaptic refractory effects are modeled with a simple absolute refractory period and a short exponential relative refractory period. The model does not include any of the postsynaptic effects associated with the lateral olivo-cochlear efferent system.

The restriction of phase locking in mammals to low-frequency signals is an important characteristic of the AN response (Kiang *et al.*, 1965). Much of the restriction is thought to originate with the low-pass filtering of the IHC membrane (Palmer and Russell, 1986). Unfortunately, the decline of phase locking in the Meddis (1986) IHC was erroneously modeled as an exclusive function of transmitter recycling processes. Moreover, some phase locking in the model persisted above 5 kHz. Some models have addressed this issue with simple low-pass filtering (Carney, 1993; Robert and Erikson, 1999), while others (Schoonhoven *et al.*, 1997; Lopez-Poveda *et al.*, 1998) have adapted biophysical models of membrane filtering. Presynaptic calcium channels have also been implicated in the restriction of AN phase locking (Kidd and Weiss, 1990). In the present model, phase locking is restricted to low frequencies by a combination of low-pass filtering of the RP, the dynamics of calcium flow, and transmitter recycling.

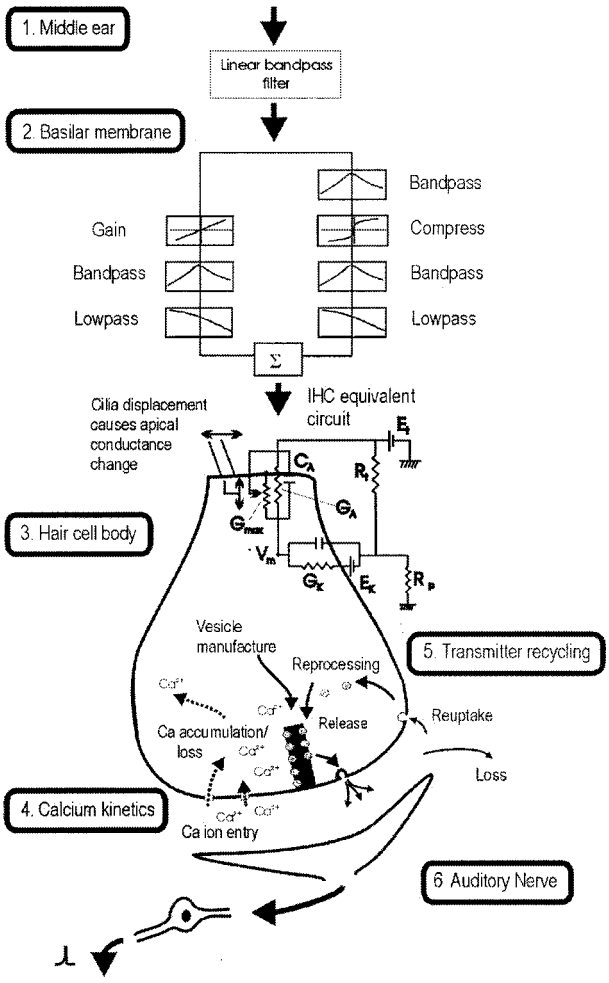

FIG. 1. Schematic diagram of the complete composite auditory model.

II. THE IHC MODEL

The input to the IHC model is motion of the cochlear partition, and its output is a stream of transmitter release events. However, a full evaluation of the model requires assumptions concerning the middle and inner ear as well as the functioning of AN fibers. The details of the IHC model are described in this section, while the supportive stages required for modeling are presented in Sec. III. Figure 1 shows the complete processing path for the model, from sound entering the auditory canal to spiking on the auditory nerve.

A. IHC receptor potential

The model incorporates a modified version of the simulation by Shamma *et al.* (1986) of the transduction of BM motion into RP. The displacement of the IHC cilia, $u(t)$, as a function of BM velocity, $v(t)$, is given by

$$\tau_c \frac{du(t)}{dt} + u(t) = \tau_c C_{\text{cilia}} v(t), \tag{1}$$

where C_{cilia} is a gain factor and τ_c is a time constant. Thus, cilia move in phase with BM velocity at low frequencies and with displacement at high frequencies. The cilia displace-

ment causes a change in the number of open ion channels and, consequently, in the apical conductance $G(u)$. The total apical conductance is given by

$$G(u)=G_{\text{cilia}}^{\max}\left[1+\exp\left(-\frac{u(t)-u_0}{s_0}\right)\times\left[1+\exp\left(-\frac{u(t)-u_1}{s_1}\right)\right]\right]^{-1}+G_a, \quad (2)$$

where $G_{\text{cilia}}^{\max}$ is the transduction conductance with all channels open, and G_a is the passive conductance in the apical membrane. The proportion of open channels is modeled as a three-state energy barrier (Boltzmann) function (see Mountain and Hubbard, 1996), where s_0, u_0, s_1, and u_1 are constants determining the exact shape of the nonlinearity. These are chosen to fit cilia displacement-depolarization functions (Russell *et al.*, 1986). Equation (2) replaces a first-order Boltzmann function employed by Shamma *et al.* The membrane potential of the cell body is modeled with a passive electrical circuit analog (Fig. 1, module 3), described by

$$C_m\frac{dV(t)}{dt}+G(u)(V(t)-E_t)+G_k(V(t)-E_k')=0, \quad (3)$$

where $V(t)$ is the intracellular hair cell potential; C_m is the cell capacitance; G_k is the voltage-invariant basolateral membrane conductance; E_t is the endocochlear potential; and $E_k'=E_k+E_tR_p/(R_t+R_p)$ is the reversal potential of the basal current E_k (mostly potassium; Corey and Hudspeth, 1983), corrected for the resistance (R_t,R_p) of the supporting cells (see Shamma *et al.*, 1986).

B. Calcium controlled transmitter release function

The release of neurotransmitter into the synaptic cleft is mediated by calcium ions in all synapses. Augustine *et al.* (1985a) showed that postsynaptic potentials were only observed when presynaptic depolarization coincided with the presence of extracellular Ca^{2+} (see Johnston and Wu, 1995, for a review). The transmitter release function is a three-part process, labeled as module 4 in Fig. 1.

1. Depolarization of the IHC membrane leads to the opening of calcium ion channels

We employ a third-order process similar to Hudspeth and Lewis (1988) and Kidd and Weiss (1990), but with a time constant that is not voltage dependent. Calcium current (I_{Ca}) is a function of the RP

$$I_{\text{Ca}}(t)=G_{\text{Ca}}^{\max}m_{I_{\text{Ca}}}^3(t)(V(t)-E_{\text{Ca}}), \quad (4)$$

where E_{Ca} is the reversal potential for calcium and $G_{\text{Ca}}^{\max}$ is the calcium conductance in the vicinity of the synapse, with all the channels open. $m_{I_{\text{Ca}}}(t)$ is the fraction of calcium channels that are open. The steady-state value of the latter, $m_{I_{\text{Ca}},\infty}$, is modeled by a Boltzmann function

$$m_{I_{\text{Ca}},\infty}=[1+\beta_{\text{Ca}}^{-1}\exp(\gamma_{\text{Ca}}V(t))]^{-1}, \quad (5)$$

where β_{Ca} and γ_{Ca} are constants chosen to reflect published observations of calcium currents (see Table II), and $m_{I_{\text{Ca}}}(t)$ is a low-pass-filtered function of $m_{I_{\text{Ca}},\infty}$

$$\tau_{I_{\text{Ca}}}\frac{dm_{I_{\text{Ca}}}(t)}{dt}+m_{I_{\text{Ca}}}(t)=m_{I_{\text{Ca}},\infty}, \quad (6)$$

where $\tau_{I_{\text{Ca}}}$ is a time constant.

2. Calcium ions enter the cell, and accumulate briefly in the vicinity of the synapse

Calcium concentration $[Ca^{2+}](t)$ is modeled as a first-order, low-pass-filtered function of calcium current, $I_{\text{Ca}}(t)$ (after Hudspeth and Lewis, 1988)

$$\tau_{[\text{Ca}]}\frac{d[Ca^{2+}](t)}{dt}+[Ca^{2+}](t)=I_{\text{Ca}}(t), \quad (7)$$

where $\tau_{[\text{Ca}]}$ is a time constant.

3. The probability of the release of transmitter is proportional to the cube of Ca^{2+} concentration

We employ the function

$$k(t)=\max(([Ca^{2+}]^3(t)-[Ca^{2+}]_{\text{thr}}^3)z,0), \quad (8)$$

where $[Ca^{2+}]_{\text{thr}}$ is a threshold constant, z is a scalar for converting calcium concentration levels into release rate, and the cube function is based on data by Augustine *et al.* (1985b).

C. Quantal and probabilistic model of synaptic adaptation

The transmitter release rate, $k(t)$, drives a model of synaptic adaptation identical to that given in Lopez-Poveda *et al.* (1998). It simulates the functional characteristics of adaptation, which are assumed here to be due to presynaptic transmitter depletion. The scheme is the same as that proposed by Meddis (1986) except that release of transmitter into the cleft is now quantal and stochastic. It is described by the following equations:

$$\frac{dq(t)}{dt}=N(w(t),x)+N([M-q(t)]y)-N(q(t),k(t)), \quad (9)$$

$$\frac{dc(t)}{dt}=N(q(t),k(t))-lc(t)-rc(t), \quad (10)$$

$$\frac{dw(t)}{dt}=rc(t)-N(w(t),x). \quad (11)$$

Figure 1, module 5, shows one possible physical interpretation of this system. Individual vesicles of neurotransmitter (probably glutamate), are released from the *immediate* (q) store into the *cleft* (c), at a rate, $k(t)$, that is dependent on calcium concentration. In the cleft, the transmitter disperses and some is lost from the system at a rate l. The remaining transmitter in the cleft is taken back into the cell into a *reprocessing* (w) store at a rate r. Here, it is repackaged into vesicles that are returned to the immediate store at a rate x. Additionally, q is continuously replenished with new transmitter vesicles at a rate, $y[M-q(t)]$, where M represents the maximum number of transmitter quanta that can be held in the immediate store (q).

Neurotransmitter in the immediate store is quantal, and enters and leaves stochastically. The stochastic transport of neurotransmitter is described by the function $N(n,\rho)$, in which each of n quanta has an equal probability of release, ρdt, in a single simulation epoch. In the cleft and reprocessing stores, transmitter is a continuous quantity. This means, for instance, that the contents of the reprocessing store must be an integer number greater than 1 for a transmitter quantum to be eligible to rejoin the immediate store. The output from the synapse is a stream of discrete events indicating vesicle releases, $N(q(t),k(t))$. More detailed accounts of this process in a nonstochastic form can be found in Meddis (1986, 1988), Meddis *et al.* (1991) and Hewitt and Meddis (1991).

III. INPUT TO AND OUTPUT FROM THE IHC

Very few studies apply stimuli directly to, or record directly from, IHCs. As a consequence, full evaluation of our IHC algorithm requires that we simulate both the proximal stimulus (BM velocity) in response to acoustic stimuli and the typical response in AN fibers. To do this we need supplementary models. In our evaluation we have used a model of the low- and high-frequency attenuation of the middle ear (Sec. III A) and a nonlinear filtering operation to represent the motion of the BM (Sec. III B). Section III C describes the procedure used to simulate the conversion of release events into APs in the AN itself.

A. Middle ear

The response of middle ear is modeled by a second-order linear bandpass Butterworth filter with an upper cutoff of 22 kHz and a lower cutoff of 12.5 kHz. This was to fit to data from a single guinea-pig middle ear at high frequencies (Nuttall and Dolan, 1996). The input to the filter is sound pressure (μPa) and the output is stapes velocity, $x(t)$, in m/s. This transformation was achieved with a scale factor of 1.4 $\times 10^{-10}$ ms^{-1} μPa^{-1}.

B. DRNL cochlear filtering

The filtering of the BM is modeled with a "dual-resonance-nonlinear" (DRNL) filter architecture which has been described and evaluated more fully elsewhere (Meddis *et al.*, 2001). The input to the DRNL is stapes velocity and the output is BM velocity, $v(t)$. Figure 1, module 2, shows the basic architecture. A single DRNL filter consists of two parallel pathways, one linear and the other nonlinear, whose outputs are summed to produce the filter output. The linear pathway is a gammatone filter (Patterson *et al.*, 1988) followed by a low-pass filter and a gain. The nonlinear pathway consists of the following cascade: a gammatone filter, a compression function, a second gammatone filter, and a low-pass filter. The compression in the nonlinear pathway is described by

$$y[t]=\text{sign}(x[t])\times\min(a|x[t]|,b|x[t]|^{\nu}), \tag{12}$$

where a, b, and ν are parameters of the model that vary as a function of location along the partition. The DRNL parameters are initially fitted to guinea-pig BM laser-interferometry data at a site with a BF of 18 kHz (Nuttall and Dolan, 1996), as described by Meddis *et al.* (2001).

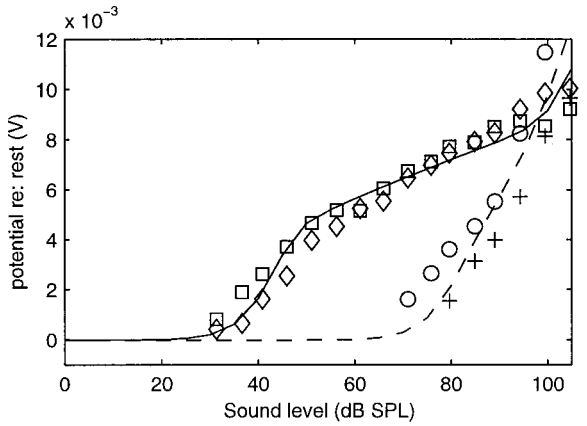

FIG. 2. dc receptor potential. Unconnected symbols are animal data recorded from IHC with 18-kHz BF (Patuzzi and Sellick, 1983), using 7-kHz stimulus (+, ○) and 18-kHz stimulus (□, ◇). Continuous lines are the model response at 7 kHz (dashed) and at 18 kHz (solid).

C. AN response

Postsynaptic intracellular recordings from the dendrites of guinea-pig AN bipolar neurons suggest that the release of a single quantum of transmitter is sufficient to produce an AP in an AN fiber, at least when the fiber is in a nonrefractory state (Siegel, 1992). The input to the AN stage of the model is a stream of transmitter release events from the synapse. Refractoriness (both absolute and relative) is simulated by a uniform random process. For each vesicle release, an AP is generated in the fiber if a vesicle is released and $p(t)$ exceeds a random number (0–1)

$$P(t)=0, \quad \text{for } (t-t_l)<R_A \tag{13}$$
$$p(t)=1-c_r e^{-(t-t_l-R_A)/s_r}, \quad \text{for } (t-t_l)\geq R_A,$$

where c_r is 0.55 and determines the maximum contribution of the relative refractory period in $p(t)$; s_r is 0.8 ms, and is the time constant of refraction; t is time now, t_l is the time of the last spike, and R_A is 0.75 ms, the absolute refractory period.

IV. MODEL EVALUATION

The implementation of the complete peripheral model described in Secs. II and III was fitted to high-BF guinea-pig data, at the level of the RP and the AN. All computations were by numerical integration and used a time step of 10 μs. Since the model is inherently stochastic, repeated runs (between 20 and 500) are required to build up reliable post-stimulus time histograms (PSTHs). The implementation was developed using the Development System for Auditory Modeling (DSAM) C libraries.[1]

A. Average rate responses

1. dc component of the receptor potential

The average response to high-frequency stimulation in the IHC is measured as the dc component of the intracellular potential. Unconnected symbols in Fig. 2 show the dc RP of

TABLE I. IHC receptor potential [Eqs. (1), (2) and (3)].

Et, endocochlear potential (V)	$100E-3$
Ek, potassium reversal potential (V)	$-70.45E-3$
*G*0, resting conductance (S=Siemens)	$1.974E-9$
Gk, potassium conductance (S)	$1.8E-8$
E_k correction, $Rp/(Rt+Rp)$	0.04
$G_{\text{cilia}}^{\max}$, max. mechanical conductance (S)	$8E-9$
s_0, displacement sensitivity (m^{-1})	$85E-9$
u_0, displacement offset (m)	$7E-9$
s_1, displacement sensitivity (m^{-1})	$5E-7$
u_1, displacement offset (m)	$7E-9$
C_m, total capacitance (F)	$6E-12$
τ_c, cilia/BM time constant (s)	$2.13E-3$
C_{cilia}, cilia/BM coupling gain (dB)	16

the guinea-pig IHC (Patuzzi and Sellick, 1983), in response to pure-tone stimulation at BF (18 kHz) and off-BF (7 kHz). The two functions have a different shape. This is likely to reflect differences between the compressed response of the BM to stimulation at BF and linear response at frequencies well below BF. The solid and dashed lines show the response of the model at the two stimulus frequencies. The threshold of the animal BF response is higher than often found in AN measurements, which may indicate a loss of tip sensitivity in the animal preparation. To fit these responses, at both stimulus frequencies, required different DRNL parameters from those used by Meddis *et al.* (2001). The new parameters are given in Table III as ''IHC set.'' With an appropriate choice of IHC parameters, cilia coupling gain, C_{cilia}, and mechanically driven conductance, $G_{\text{cilia}}^{\max}$ [Eqs. (1) and (2)], it was possible to engineer an almost-perfect fit between the animal and model data. These are given in Table I.

2. Rate-intensity functions of the AN

In guinea pigs, RI functions at BF have been divided into three categories (Winter *et al.*, 1990). HSR fibers display activity in the absence of any stimulus (SR >18 spikes/s), have a low acoustic threshold ($<$20-dB SPL in the data used here), and a steep RI function at BF that almost completely saturates within 20–30 dB of the threshold. MSR fibers (SR<18 spikes/s) display a ''sloping saturation'' type rate of growth at BF. LSR fibers have almost no spontaneous activity, have high thresholds, and display an RI function at BF with a shallow slope. These different shapes are thought to reflect the linear and compressive regions of BM response (Yates *et al.*, 1990). Figure 3 compares model results with two AN RI functions at BF for each fiber type (from Winter *et al.*, 1990). They all use the same DRNL parameter set (''AN set'' Table III; see below for their derivation). The RP parameters used were the same as in Sec. IV A 1. Only three transmitter release parameters, $G_{\text{Ca}}^{\max}$, $[\text{Ca}^{2+}]_{\text{thr}}$, and *M*, were varied to produce the six model functions (see Table II, columns H_1, H_2, M_1, M_2, L_1, L_2).

It was a weakness of earlier models (e.g., Meddis and Hewitt, 1991; Carney, 1993) of hair-cell functioning that they were unable to model the change in shape of the RI function when frequencies different from BF were used. Figures 4(A) and (C) show examples of RI functions measured both at BF (16 kHz), and at frequencies above and below BF

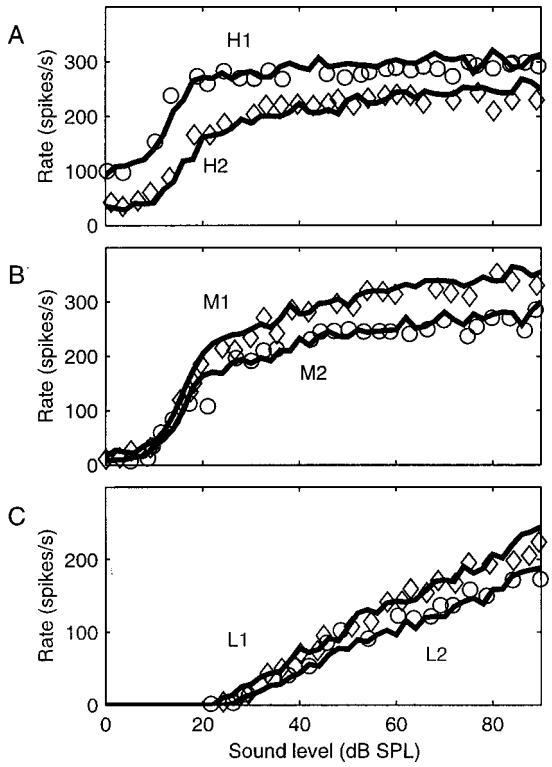

FIG. 3. AN rate-intensity responses for different fiber types. Unconnected symbols are animal data (Winter *et al.*, 1990). Solid lines are responses of the model. All fits employ the same DRNL parameters (''AN set''; Table III). Variation in synapse parameter values is shown explicitly in Table II.

[Yates *et al.*, 1990; Figs. 2(A) and 3(A)]. Both fibers are from the same guinea pig. In Fig. 4(A), a BF stimulus results in a typical HSR saturating function with a narrow dynamic range. However, when stimuli at other frequencies are used, the RI function for the same fiber can be either sloping saturation (19 kHz) or saturating (12 kHz). Yates *et al.* (1990) propose that this is due in part to the BM response, which is nonlinear at BF but linear away from BF. The DRNL filter used in this evaluation was designed to simulate this effect. Figure 4(C) shows the response of an MSR fiber from the same animal with a similar BF ($\sim$16 kHz). Figures 4(B) and (D) show the model RI response to BF and off-BF tones. Both fiber responses use the same DRNL parameters (see Table III, ''AN set'') that were chosen specifically for these data. The difference between the two figures arises from changes to calcium control parameters $G_{\text{Ca}}^{\max}$ and $[\text{Ca}^{2+}]_{\text{thr}}$. These values are given in Table II [columns labeled HSR and MSR for Figs. 4(B) and (D), respectively]. The good agreement between the model and the data indicates that it is possible to simulate important characteristics of different fiber types in terms of differences in synapse parameters.

3. The influence of the transmitter release function on fiber type

Figure 5(A) shows how model RI functions vary when the maximum calcium conductance parameter, $G_{\text{Ca}}^{\max}$, is varied. Other parameters are the same as those for the model shown in Fig. 4(A). As conductance increases, the function changes from ''straight'' to ''sloping saturation,'' and finally

TABLE II. IHC synapse calcium channels and transmitter release [Eqs. (4–11)].

z, scalar $(s*[Ca^{2+}]^3)^{-1}$	20×10^{31}
E_{Ca}, reversal potential (V)	0.066
β_{Ca}	400
γ_{Ca}	130
τ_m, calcium current time constant (s)	1×10^{-4}
τ_{Ca}, calcium diffusion time constants (s)	1×10^{-4}
y, replenishment rate (s^{-1})	10
l, loss rate (s^{-1})	2580
x, reprocessing rate (s^{-1})	66.3
r, recovery rate (s^{-1})	6580

Fiber ID	HSR	MSR	H_1	H_2	M_1	M_2	L_1	L_2
G_{Ca}^{max}, max. Ca^{2+} conductance (nS)	8	4.5	7	4.5	4	4.25	2.75	2.75
$[Ca^{2+}]_{thr}(\times10^{-11})$, threshold Ca^{2+} conc.	4.48	3.2	2	0	2	2.5	4	4.2
M, max. free transmitter quanta	10	10	10	8	13	9	8	6

to ''saturating.'' At the same time, the threshold drops, the spontaneous rate increases, and the synapse saturates at lower stimulus intensities. Calcium conductance alone seems to determine, at least qualitatively, the full range of RI function types, spontaneous rates, and thresholds described in the literature.

The effect of varying $[Ca^{2+}]_{thr}$, for two different values of G_{Ca}^{max}, corresponding approximately to low- and high-spontaneous rate responses, is shown in Fig. 5(B). $[Ca^{2+}]_{thr}$ imposes a threshold calcium concentration for transmitter release [Eq. (8)] and affects the response mainly at low intensities. Therefore, it is not possible to model the observed range of fiber characteristics by changing $[Ca^{2+}]_{thr}$ alone. However, we have used $[Ca^{2+}]_{thr}$ in the preceding figures to improve the exact fit to the data beyond that possible using G_{Ca}^{max} alone (particularly in defining the precise threshold of LSR fibers). The effect of varying the maximum number of vesicles available for immediate release, M, for two different values of G_{Ca}^{max} is shown in Fig. 5(C). The only effect of M is to scale the release rate linearly across the entire dynamic range. Therefore, M alone cannot account for differences in fiber type. A larger value of M can be helpful in fitting MSR and LSR responses, as it increases the firing rate, without driving the synapse into saturation. M is 13 or less in all cases.

B. Phase locking

The ability of the transduction apparatus to follow, cycle-by-cycle, a stimulus waveform, in all mammals, falls

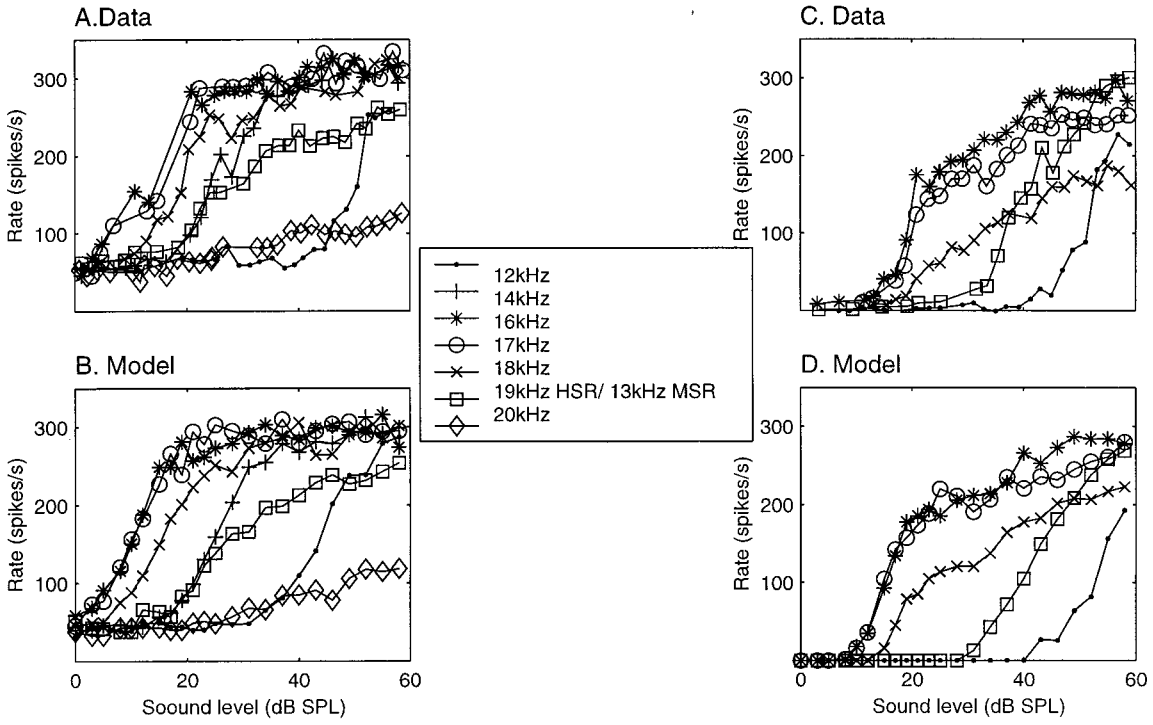

FIG. 4. Rate-intensity responses of AN fibers both at BF and off-BF. (A) HSR fiber from Yates *et al.* (1990). (B) Response of model using the ''AN set'' DRNL parameters (Table III) and ''HSR'' synapse parameters ($G_{Ca}^{max}=8\times10^{-9}$,$[Ca^{2+}]_{thr}=4.48\times10^{-11}$,$M=10$). (C) MSR fiber from Yates *et al.* (1990). (D) Response of model using the ''AN set'' DRNL parameters and ''MSR'' synapse parameters ($G_{Ca}^{max}=4.5\times10^{-9}$,$[Ca^{2+}]_{thr}=3.2\times10^{-11}$,$M=10$).

TABLE III. Basilar-membrane filtering (DRNL) parameters [Eq. (12)].

	IHC set	AN set
Center frequency of nonlinear path (Hz)	17 300	16 700
Bandwidth (Hz) of nonlinear path (Hz)	1 200	3 730
Gamma-tone filter cascade of nonlinear path	3	4
Low-pass filter cascade of nonlinear path	3	2
a, compression parameter	3 000	18 000
b, compression parameter	0.06	7.8×10^{-3}
ν, compression parameter	0.25	0.16
Center frequency linear path (Hz)	13 700	12 900
Bandwidth of linear path (Hz)	1 400	800
Gamma-tone filter cascade of linear path	2	2
Low-pass filter cascade of nonlinear path	4	3
Linear path gain	720	780

off with frequency. In the guinea pig, the decay is rapid above 1–2 kHz. Here, we compare the model response to the RP and AN observations of Palmer and Russell (1986).

1. ac/dc ratios of the receptor potential

Phase locking in the hair cell can be measured by the ratio of the peak-to-trough magnitude of the intracellular potential, to its dc displacement from rest. Figure 6(A) compares the data of Palmer and Russell (various symbols) with the response of the model (solid line). Palmer and Russell

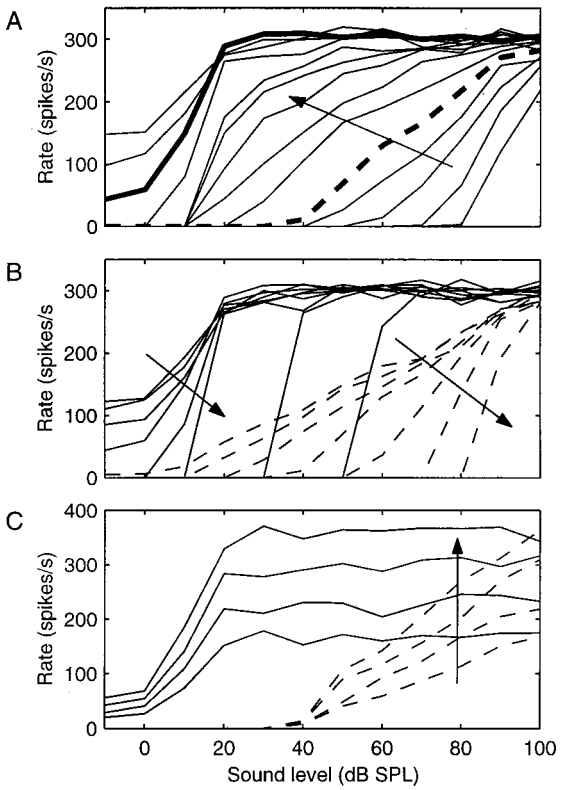

FIG. 5. Effect of varying synapse parameters on rate-intensity functions, starting from the ''HSR'' synapse values (Table II). The ''AN set'' (Table III) DRNL parameters were used. (A) The effect of increasing G_{Ca}^{max}, from 1.5 to 10 nS in the direction of the arrow. Thick solid line is for $G_{Ca}^{max}=8$ nS and thick dashed line is for $G_{Ca}^{max}=2.5$ nS. (B) The effect of increasing $[Ca^{2+}]_{thr}$ from zero to 18×10^{-11} in the direction of the arrows, for two different values of G_{Ca}^{max} (2.5 nS for dotted lines and 8 nS for solid lines). (C) The effect of increasing M from 5 to 13 in the direction of the arrows, for the same two values of G_{Ca}^{max} as (B) (for $[Ca^{2+}]_{thr}=4.48\times10^{-11}$).

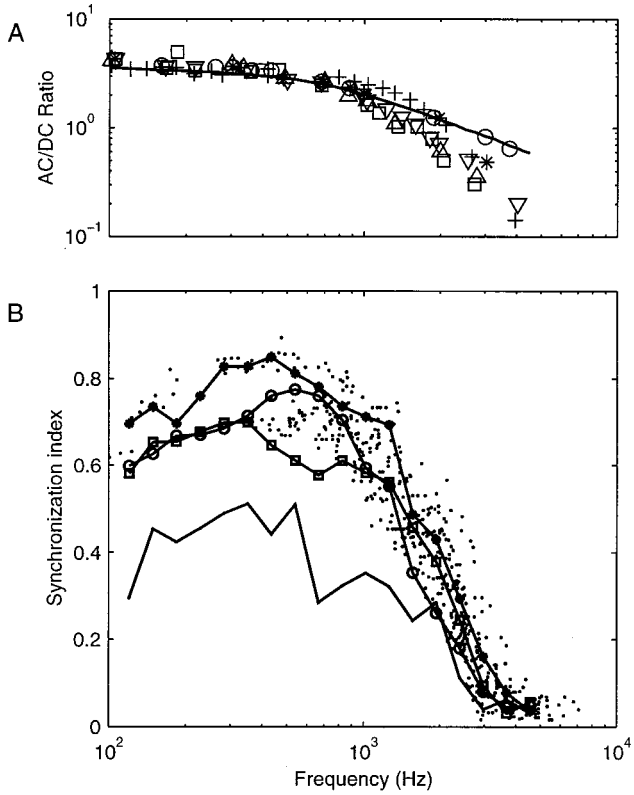

FIG. 6. Phase-locking. (A) Receptor potential ac/dc ratio. Unconnected symbols are several datasets from the guinea pig data (Palmer and Russell, 1986); the solid line is the response of the model. The DRNL parameters used are given in Table III, ''IHC set.'' (B) The synchronization index at the AN. Unconnected dots are guinea-pig data and the solid lines are model responses at four signal levels (——10 dB; □ 0 dB, ● 20 dB, ○ 40 dB SL). The model uses the ''HSR'' synapse values (Table II) and the ''AN set'' (Table III) DRNL parameters.

(1986) used low-frequency pure-tone stimuli (<5 kHz) at 80 dB SPL, and recorded from high-BF (>15 kHz) IHCs. It was necessary to change the low-frequency cutoff of the model middle-ear response down to 500 Hz, in order for the model to produce large enough output at this level. Such an action is supported experimentally. Even a small hole in the bulla, as used in these experiments to equalize middle-ear pressure and allow monitoring of the compound action potential, causes a strong increase in response at low frequencies (Ruggero *et al.*, 1990). The value of the membrane capacitance of the cell, C_m, was set to 6 pF, to produce the correct ac/dc ratios. This is close to the experimental findings of Russell and Sellick (1978), who found whole-cell capacitances in the range 8–16 pF, and Kros and Crawford (1990), who estimated values of 6–13 pF. The model gives a reasonable fit, although the slope is shallow compared with most of the data sets. The model used the DRNL parameter set shown in Table III under ''IHC set,'' and the RP stage parameters shown in Table I.

2. Synchronization index in the AN

The synchronization index (SI; Johnson, 1980), a measure of phase locking, is given in Fig. 6(B) for the data of Palmer and Russell (1986) and the model of Fig. 4(B). The model used the DRNL parameter set shown in Table III under ''AN set,'' the RP stage parameters shown in Table I, and

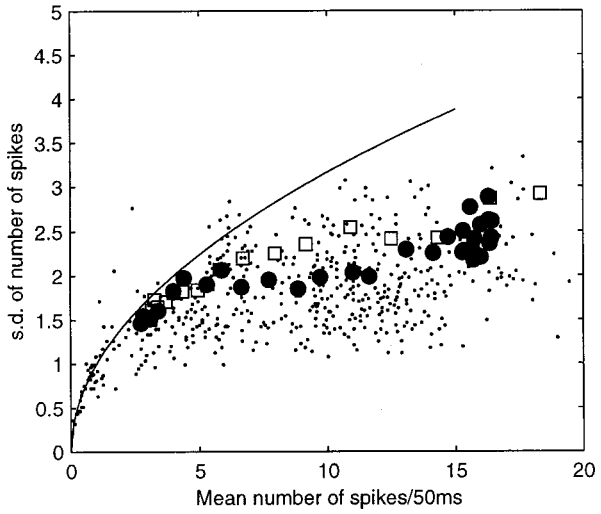

FIG. 7. The relationship of mean to variance in AN firing rate for 50-ms tone pips as measured by Winter and Palmer (1991). Small dots are the data of Winter and Palmer; solid circles are the behavior of the model using the "AN set" DRNL parameters (Table III) and "MSR" synapse parameters (Table II). Open squares are the response of this model without the explicit absolute and relative refractoriness of Sec. III C.

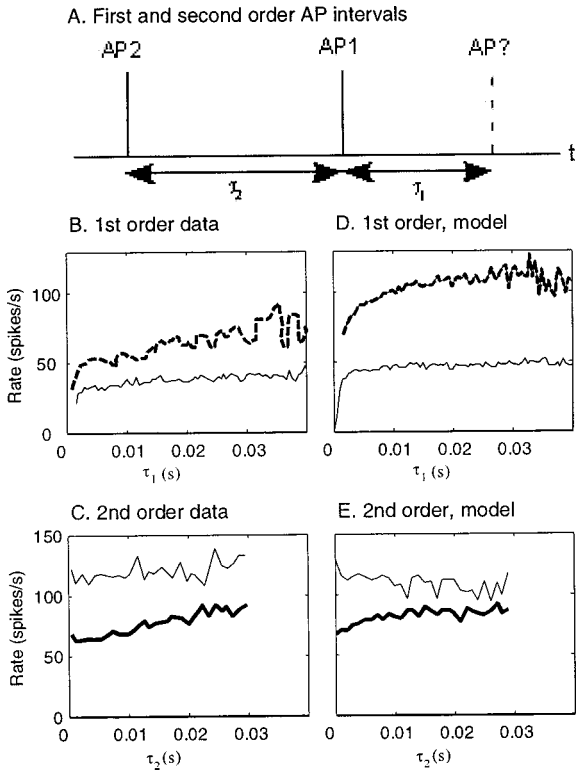

FIG. 8. AN discharge history effects. (A) Cartoon of APs showing first- and second-order intervals. Solid bars (AP1 and AP2) are spikes that have already occurred and the dashed bar is a possible spike (AP?) at the instant τ_1 after the immediately preceding spike AP1. (B) First-order hazard functions derived from spontaneous APs of cat from Gaumond *et al.* (1982, thin solid line) and Grey (1967, thick dashed line). τ_1 is the time interval between two APs. (C) Second-order hazard functions from Gaumond *et al.* τ_2 is the time interval between the preceding spike (AP1) and the spike before it (AP2). The thick line shows the hazard function based on short values of τ_1 between 1 and 4 ms. The thin line is based on longer intervals, τ_1 between 20 and 40 ms. (D) First-order hazard function for spontaneous activity of the model. The thin solid line uses the "AN set" DRNL parameters (Table III) and "HSR" synapse parameters (Table II). The thick dashed line uses the modified model (see the text). (E) Second-order hazard functions for the modified model fiber of (D), for comparison with (C).

"HSR" synapse parameters in Table II. The time constants for calcium influx, τ_m, and accumulation, τ_{Ca}, were both set to 0.1 ms. These values produced a good fit to the data, and are consistent with the results of Hudspeth and Lewis (1988). The animal phase-locking measurements were made in fibers having BFs below 9 kHz. We used a high BF in these simulations and, as a consequence, the sound level required is considerably higher. However, with small exceptions, there is a good fit between the model results for 20-dB SL. The thresholds vary from 85–110 dB SPL. At these frequencies, the output from the DRNL is linear, so the comparison is valid despite the high sound levels. The effect of sound level on SI is not shown by any animal data here. Qualitatively, Palmer and Russell noted that SI rises with level, is often detectable below threshold, and reaches a maximum within 20 dB above threshold. Above that, they found that SI sometimes decreases slightly. Figure 6(B) shows the model response from −10 to 40-dB SL. The behavior of the model conforms to Palmer and Russell's findings. The changes in SI with sound level in the model are a consequence of the fact that random spontaneous activity compromises phase locking at low signal levels. At very high levels, the signal is above threshold for a greater fraction of its period, thus reducing the SI.

C. Spike statistics

1. Mean-to-variance of firing rate

A number of studies have been made of the relationship between the mean firing rate and its variance (e.g., Teich and Khanna, 1985; Young and Barta, 1986; Winter and Palmer, 1991). At higher firing rates the variance is less than the mean, indicating a departure from the prediction of a Poisson model of spiking statistics. The difference is often accounted for by introducing a simple refractory stage (e.g., Young and Barta, 1986). Figure 7 shows the mean-variance relationship measured by Winter and Palmer (1991) in the guinea pig (small dots). A clear departure from the Poisson prediction (solid line) is evident. The large solid circles represent the behavior of the model for the MSR fiber (the HSR model could not be used for measurements at spike rates below its SR), applied to stimulus paradigm described by Winter and Palmer. The model agrees well with the data, considering that no attempt was made to tune the model for this demonstration. The output of the model is also plotted with the AN refractory module removed (open squares). There is still considerable departure from the Poisson prediction with the synapse alone.

2. Discharge history effects

During steady-state activity, the instantaneous rate of firing of AN fibers is depressed immediately after an AP (first-order effects) and further depressed if two APs follow in rapid succession (second-order effects). Figure 8(A) shows this. First-order effects can be quantified, using hazard functions[2] that estimate the probability of an AP [AP? in Fig. 8(A)] as a function of the interval, τ_1, since the last spike

AP1. The animal hazard functions of spontaneous activity in Fig. 8(B) (Grey, 1967; thick dashed line; Gaumond *et al.*, 1982; thin solid line) show a depression in firing rate following short interspike intervals (small τ_1) that recovers over a 30-ms period. However, as shown in Fig. 8(B), the magnitude of the effect varies between observations. Second-order discharge history effects can be quantified as the probability of a spike, AP?, as a function of the interval, τ_2, between the preceding spike, AP1, and the one before that, AP2 [see Fig. 8(A)]. This is normally calculated as an average across a given range of the interval, τ_1. Figure 8(C) shows two hazard series based on a long train of spontaneous APs (Gaumond *et al.*, 1982), where each series is expressed as a function of the preceding interspike interval, τ_2. The thick line deals with very short first-order intervals ($1<\tau_1<4$ ms), while the thin line deals with longer intervals ($20<\tau_1<40$ ms). The firing rate is depressed most when short first-order interspike intervals (τ_1, thick line) are combined with short preceding second-order intervals (low values of τ_2).

Discharge-history effects can also be seen in the working of the model where it is caused by transmitter depletion. A similar analysis of a train of spontaneous APs from the model is shown in Figs. 8(D) and (E). In the standard HSR AN model, first-order effects [Fig. 8(D), thin solid line] are very small, except for the first few milliseconds, which are dominated by AN refractory effects [Eq. (13)]. The first-order effects for longer intervals are nonetheless consistent with Gaumond *et al.*'s data in Fig. 8(B) (thin solid line). Second-order effects (not shown) are similarly small. The thick dashed line in Fig. 8(D) shows the first-order effects with the model parameters modified to increase discharge history effects. This model shows a trend more similar to that of Grey's data [thick dashed line in Fig. 8(B)]. The spontaneous rate of the model fiber was increased by setting $G_{\mathrm{Ca}}^{\max}$ to 11 nS in combination with a reduction in the maximum number of available transmitter vesicles, M, to 5. This latter value is important because the loss of a single vesicle from the immediate store, $q(t)$, represents a substantial fall in the probability of a succeeding action potential when $q(t)$ is already small. Figure 8(E) shows the second-order effects of the modified model. The model results are comparable with the animal data.

V. DISCUSSION

The model is intended to act as one module in a much larger system. Its success as a computational tool, therefore, depends primarily on the range of IHC phenomena that can be simulated. It has been shown that the model successfully reproduces the BF-tone RI functions for all three fiber types (HSR, MSR, LSR), and most of the responses to stimuli away from BF. We note that Jackson and Relkin (1998) have found that AN fiber saturated rates drop with increasing stimulus frequency above BF. The model has not reproduced this effect. It successfully reproduces correct phase-locking characteristics at the level of both the RP and the AN; the departure of AN spiking statistics from the Poisson prediction, and first- and second-order discharge-history effects. There are a number of other phenomena that have not been tested here. Adaptation has been the focus of earlier studies (Meddis, 1986, 1988). Differences of adaptation with fiber type will be a topic of future study. The response to broadband signals and, notably, two-tone suppression (2TS), is thought to have its origin in the BM. An evaluation of the DRNL filter can be found elsewhere (Meddis *et al.*, 2001). Two-tone suppression will be reported elsewhere.

The varied scope of modeling in the auditory periphery makes meaningful comparisons between models difficult. This is especially true of older models. Perhaps the closest of the recent complete peripheral models are those of Zhang *et al.* (2001) and Robert and Erikson (1999). These achieve many of the same things for the cat as we do for the guinea pig. As computational tools, all are very effective. However, our approach to the task differs. This study concentrates on the development a detailed IHC model. Zhang *et al.* and Robert and Erikson focused on two-tone suppression while we have not. We have evaluated the IHC model only for a high-BF site (~18 kHz). The choice of high BFs was decided by the excellent availability of data for the guinea pig. At low BFs, data are less complete, and the contributions of mechanical and biophysical nonlinearities are not as well understood. Nevertheless, there is no strong reason to suppose that IHCs differ substantially in their response along the partition. A complete filterbank will be described elsewhere. Our preferred strategy was to simulate, whenever known, the underlying component physiological processes in the hope that this would lead to better overall performance. A notable success in this respect is the spiking statistics arising from the stochasticity of the synapse.

Our model is most similar to the IHC models of Lopez-Poveda *et al.* (1998) and Schoonhoven *et al.* (1997). They both employed *ad hoc* transmitter release control functions, while, in this study, we have taken a further step, and introduced a model of calcium control of transmitter release. The differences in the model between HSR, MSR, and LSR AN fibers are attributed largely to differences in the presynaptic maximum calcium conductance ($G_{\mathrm{Ca}}^{\max}$). No other parameter had this effect. The characteristics of the calcium current are based on physiological observations, and it seems reasonable that transmitter release will be affected if the number of calcium channels vary. However, the model can only establish the feasibility of this mechanism. The calcium model is very simple and it is possible that other mechanisms not known or not included in the model (e.g., calcium buffering) may be responsible for fiber-type differences. For example, it has been suggested that different calcium channel types may underlie the differences between fiber types (Zhang *et al.*, 1999). Mechanisms might also be postsynaptic (e.g., Geisler, 1981). Very recently, Puel (2001) has demonstrated that efferents synapsing onto the dendrites of the AN regulate SR, thresholds, and dynamic range of AN fibers via tonic inhibition.

The use of two cubed functions in the transmitter release function produces a ninth-order function of sound level [Eq. (4) and Eq. (8)]. This may appear to contradict some experimental data, showing that dc RP and AN firing obeys square-law behavior near to threshold (Dallos, 1985; Müller *et al.*,

1991). However, the functions employed for the calcium processes are themselves based on experimental data (Augustine *et al.*, 1985a, b). These functions do not hamper the model for the RP or AN data shown here, it remains an issue to be resolved.

In a modeling study, Kidd and Weiss (1990) found that calcium dynamics is likely to impact on IHC phase locking. Calcium dynamics plays a role in our model, but its effect on phase locking is relatively minor. Other factors, including the receptor potential and delays in the circulation of the transmitter material, also have an effect. However, our model does not allow us to draw any strong conclusion about the relative importance of calcium in phase locking. Although the AN output of the model fits the phase-locking data excellently, the fit to the RP data is not perfect. This is probably because observed voltage-dependent potassium currents (Kros and Crawford, 1990) are modeled as a passive conductance. Further research is required before we can effectively model the contribution of each process.

A new feature of our model is the location of stochasticity at the synapse. In most other models, the auditory-nerve stage is itself treated as stochastic. However, studies of isolated spiral ganglion cells (Lin, 1997; Santos-Saachi, 1993) show little evidence of stochasticity. Likewise, the required degree of stochasticity is not observed in RP recordings. In contrast to most synapses, auditory-nerve synapses have a relatively small vesicle supply (Liberman, 1980), so the stochastic release of vesicles is probably unavoidable. Employing quantal vesicle release in the model means that the value of M, the maximum number of vesicles available for release, is an important determinant of synaptic response. Small values of M, typically less than 13, are essential to give appropriate results. When modeling Gaumond *et al.*'s data (1982), it was necessary to restrict the value of M to 5 quanta in order to reproduce his pronounced second-order discharge history effects. The small number of quanta typically required for effective functioning of the model amounts, in effect, to a prediction requiring physiological confirmation when techniques for investigating individual synapses become sophisticated enough to address the issue. The synapse in the model also accounts for the majority of the observed mean-to-variance relationship. This is interesting, as it is usually attributed to the primary auditory neurons. The introduction of the stochasticity in the synapse substantially reduces the contribution of the AN refractoriness. We found, however, that the sub-1-ms effects could only be explained if the model included the 0.75-ms dead time and the additional short-term relative refractory effect.

[1]The modules employed are available in the AMS (Auditory Model Simulator) application. Both DSAM and AMS are available from http:\\www.essex.ac.uk\psychology\hearinglab\dsam

[2]This is calculated from an interspike-interval histogram. Expressed as a firing rate, it is the ratio of the number of intervals τ_1 over the number of intervals $\geqslant \tau_1$, all divided by the bin width (0.5 ms).

Augustine, G. J., Charlton, M. P., and Smith, S. J. (**1985a**). ''Calcium entry into voltage-clamped pre-synaptic terminals of squid,'' J. Physiol. (London) **367**, 143–162.

Augustine, G. J., Charlton, M. P., and Smith, S. J. (**1985b**). ''Calcium entry and transmitter release at voltage-clamped nerve terminals of squid,'' J. Physiol. (London) **367**, 163–181.

Carney, L. H. (**1993**). ''A model for the responses of low-frequency auditory-nerve fibers in cat,'' J. Acoust. Soc. Am. **93**, 401–417.

Corey, D. P., and Hudspeth, A. J. (**1983**). ''Kinetics of the receptor current in the bullfrog saccular hair-cells,'' J. Neurosci. **3**, 962–976.

Dallos, P. (**1985**). ''Response characteristics of mammalian cochlear hair cells,'' J. Neurosci. **5**, 1591–1608.

Davis, H. (**1965**). ''A model for transducer action in the cochlea,'' Cold Spring Harbor Symp. Quant. Biol. **30**, 181–189.

Eggermont, J. J. (**1985**). ''Peripheral auditory adaptation and fatigue: A model oriented review,'' Hear. Res. **18**, 57–71.

Gaumond, R. P., Molnar, C. E., and Kim, D. O. (**1982**). ''Stimulus and recovery dependence of cat cochlear nerve fiber spike discharge probability,'' J. Neurophysiol. **48**, 856–873.

Geisler, C.D. (**1981**). ''A model for discharge patterns of primary auditory-nerve fibers,'' Brain Research **212** 198–201.

Grey, P. R. (**1967**). ''Analyses of spike activity of single neurons,'' Biophys. J. **7**, 759–777.

Hewitt, M. J., and Meddis, R. (**1991**). ''An evaluation of eight computational models of mammalian inner hair-cell function,'' J. Acoust. Soc. Am. **90**, 904–917.

Hudspeth, A. J., and Lewis, R. S. (**1988**). ''Kinetic analysis of voltage- and ion-dependent conductances in saccular hair cells of the bull-frog, *rana catesbeneiana*,'' J. Physiol. (London) **400**, 237–274.

Irino, T., and Patterson, R. D. (**2001**). ''A compressive gammachirp auditory filter for both physiological and psychophysical data,'' J. Acoust. Soc. Am. **109**, 2008–2022.

Jackson, B. S., and Relkin, E. M. (**1998**). ''A frequency-dependent saturation evident in rate-intensity functions of the chinchilla auditory nerve,'' Hear. Res. **126**, 75–83.

Johnson, D. H. (**1980**). ''The relationship between spike rate and synchrony in responses of auditory-nerve fibers to single tones,'' J. Acoust. Soc. Am. **68**, 1115–1122.

Johnston, D., and Wu, S. M. (**1995**). *Foundations of Cellular Neurophysiology* (MIT University Press, Cambridge, MA).

Kiang, N. Y. S., Watanabe, T., Thomas, E. C., and Clark, L. F. (**1965**). *Discharge Patterns of Single Fibers in the Cat's Auditory Nerve* (MIT University Press, Cambridge, MA).

Kidd, R. C., and Weiss, T. F. (**1990**). ''Mechanism that degrade timing information in the cochlea,'' Hear. Res. **49**, 181–208.

Kros, C. J., and Crawford, A. C. (**1990**). ''Potassium currents in inner hair cells isolated from the guinea-pig cochlea,'' J. Physiol. (London) **421**, 263–291.

Liberman, M. C. (**1980**). ''Morphological differences amoung radial afferent fibers in the cat cochlea: An electron-microscopic study of serial sections,'' Hear. Res. **3**, 45–63.

Lin, X. (**1997**). ''Action potentials and underlying voltage-dependent currents studied in cultured spiral ganglion neurons of the postnatal gerbil,'' Hear. Res. **108**, 157–179.

Lopez-Poveda, E. A., O'Mard, L. P., and Meddis R. (**1998**). ''A revised computational inner hair cell model,'' in *Psychophysical and Physiological Advances in Hearing*, edited by A. R. Palmer, A. Rees, A. Q. Summerfield, and R. Meddis (Whurr, London), pp. 102–108.

Meddis, R. (**1988**). ''Simulation of auditory-neural transduction: Further studies,'' J. Acoust. Soc. Am. **83**, 1056–1063.

Meddis, R. (**1986**). ''Simulation of mechanical to neural transduction in the auditory receptor,'' J. Acoust. Soc. Am. **79**, 702–711.

Meddis, R., and Hewitt, M. J. (**1991**). ''Virtual pitch and phase sensitivity of a computer model of the auditory periphery. I. Pitch identification,'' J. Acoust. Soc. Am. **89**, 2866–2882.

Meddis, R., Hewitt, M., and Shackleton, T. (**1990**). ''Implementation details of a computational model of the inner hair-cell/auditory–auditory nerve synapse,'' J. Acoust. Soc. Am. **87**, 1813–1816.

Meddis, R., O'Mard, L. P., and Lopez-Poveda, E. A. (**2001**). ''A computational algorithm for computing nonlinear auditory frequency selectivity,'' J. Acoust. Soc. Am. **109**, 2852–2861.

Mountain D. C., and Hubbard, A. E. (**1996**). ''Computational analysis of hair cell and auditory nerve processes,'' in *Auditory Computation* edited by H. L. Hawkins, T. A. McMullen, A. N. Popper, and R. R. Fay (Springer, New York).

Müller, M., Robertson D., and Yates, G. K. (**1991**). ''Rate-versus-level functions of primary auditory-nerve fibers—evidence for square law behavior of all fiber categories in the guinea-pig,'' Hearing Res. **55**, 50-56.

Nuttall, A. L., and Dolan, D. F. (**1996**). ''Steady-state sinusoidal velocity responses of the basilar membrane in guinea pig,'' J. Acoust. Soc. Am. **99**, 1556–1565.
Palmer, A. R., and Russel, I. J. (**1986**). ''Phase-locking in the cochlear nerve of the guinea pig and its relation to the receptor potential of inner hair-cells,'' Hear. Res. **24**, 1–15.
Patterson, R. D., Nimmo-Smith, I., and Holdsworth, J., and Rice, P. (**1988**). ''Spiral vos final report, Part A: The auditory filterbank,'' Cambridge Electronic Design, Contract Rep. (Apu 2341).
Patuzzi, R., and Sellick, P. M. (**1983**). ''A comparison between basilar membrane and inner hair cell receptor potential input–output functions in the guinea pig cochlea,'' J. Acoust. Soc. Am. **74**, 1734–1741.
Puel, J. L. (**2001**). ''*In vivo* studies of lateral olivocochlear efferents,'' Assoc. Res. Otolaryngol. Abs: #492, 138.
Rattay, F., Gebeshuber, I. C., and Gitter, A. H. (**1998**). ''The mammalian auditory hair cell: A simple electric circuit model,'' J. Acoust. Soc. Am. **103**, 1558–1565.
Robert, A., and Eriksson, J. L. (**1999**). ''A composite model of the auditory periphery for simulating responses to complex sounds,'' J. Acoust. Soc. Am. **106**, 1852–1864.
Ruggero, M. A., Rich, N. C., Robles, L., and Shivapuja, B. G. (**1990**). ''Middle-ear response in the chinchilla and its relationship to mechanics at the base of the cochlea,'' J. Acoust. Soc. Am. **87**, 1612–1629.
Russell, I. J., and Sellick, P. M. (**1978**). ''Intracellular studies of hair cells in the mammalian cochlea,'' J. Physiol. (London) **284**, 261–290.
Russell, I. J., Cody, A. R., and Richardson, G. P. (**1986**). ''The responses of inner and outer haircells in the basal turn of the guinea-pig cochlea and in the mouse cochlea grown *in vitro*,'' Hear. Res. **22**, 199–216.
Santos-Sacchi, J. (**1993**). ''Voltage-dependant ionic conductances of type I spiral ganglion cells from the guinea pig inner ear,'' J. Neurosci. **13**, 3599–3611.
Schoonhoven, R., Prijs, V. F., and Frijns, J. H. M. (**1997**). ''Transmitter release in inner hair cell synapses: A model analysis of spontaneous and driven properties of cochlear nerve fibers,'' Hear. Res. **113**, 247–260.
Schroeder, M. R., and Hall, J. L. (**1974**). ''Model for mechanical to neural transduction in the auditory receptor,'' J. Acoust. Soc. Am. **55**, 1055–1060.
Shamma, S. A., Chadwick, R. S., Wilbur, W. J., Morrish, K. A., and Rinzel, J. (**1986**). ''A biophysical model of the cochlear processing: Intensity dependence of pure tone responses,'' J. Acoust. Soc. Am. **80**, 133–145.
Siegel, J. H. (**1992**). ''Spontaneous synaptic potentials from afferent terminals in the guinea pig cochlea,'' Hear. Res. **59**, 85–92.
Smith, R. L., and Brachman, M. L. (**1982**). ''Adaptation in auditory-nerve fibers: A revised model,'' Biol. Cybern. **44**, 107–120.
Teich, M. C., and Khanna, S. M. (**1985**). ''Pulse-number distribution for neural spike train in the cat's auditory nerve,'' J. Acoust. Soc. Am. **77**, 1110–1128.
Weiss, T. F. (**1966**). ''A model of the peripheral auditory system,'' Kybernetik **3**, 153–175.
Winter, I. M., Robertson, D., and Yates, G. K. (**1990**). ''Diversity of characteristic frequency rate-intensity functions in guinea pig auditory nerve fibers,'' Hear. Res. **45**, 191–202.
Winter, I. M., and Palmer, A. R. (**1991**). ''Intensity coding in low-frequency auditory nerve fibers of the guinea-pig'', J. Acoust. Soc. Am. **90**, 1958–1967.
Yates, G. K., Winter, I. M., and Robertson, D. (**1990**). ''Basilar membrane nonlinearity determines auditory nerve rate-intensity functions and cochlear dynamic range,'' Hear. Res. **45**, 203–220.
Young, E. D., and Barta, P. E. (**1986**). ''Rate responses of auditory nerve fibers to tones in noise near masked threshold,'' J. Acoust. Soc. Am. **79**, 426–442.
Zhang, S. Y., Robertson, D., Yates, G., and Everett, A. (**1999**). ''Role of L-type Ca2+ channels in transmitter release from mammalian inner hair cells I. Gross sound-evoked potentials,'' J. Neurophysiol. **82**, 3307–3315.
Zhang, X., Heinz, M. G., Bruce, I. C., and Carney, L. H. (**2001**). ''A phenomenological model for the responses of auditory nerve fibers. I. Nonlinear tuning with compression and suppression,'' J. Acoust. Soc. Am. **109**, 648–670.